EFFECT OF THE PORE STRUCTURE ON RESISTIVITY INDEX CURVES

M. Han[1,2], M. Fleury[1], P. Levitz[2]

[1]Institut Français du Pétrole, Rueil-Malmaison
[2]Physique de la Matière Condensée, École Polytechnique-CNRS, Palaiseau

This paper was prepared for presentation at the International Symposium of the Society of Core Analysts held in Calgary, Canada, 10-12 September, 2007

ABSTRACT

The purpose of this work is to study the influence of the pore space structure on resistivity index curves of sandstones and carbonates. We present a new method for measuring the resistivity index (RI) curve in air-brine system in drainage and imbibition. On sandstones, the results indicate a saturation exponent close to 2 in the brine saturation range S_w>20%. Below this saturation, a bending down deviation is sometimes observed. On carbonates (about 10 different structures), for single porosity granular structures, we observed quasi-linear RI-S_w curves in log-log scale with exponent *n* value of about 1.6 in drainage. For double porosity systems, there are variable results, depending on the micro-porosity configuration. For the vuggy carbonates, we observe an electrical hysteresis. These different behaviors are qualitatively explained based on NMR, SEM and X ray micro-tomography observations. At low saturation (<20%), the contribution of the water films is studied using "random walk" methods on a sphere packing. We conclude that the water film conduction has an important influence on the decrease of *n* at low saturation range.

INTRODUCTION

Water saturation in reservoir rocks is generally determined by using a power law with a default saturation exponent $n = 2$ (Archie, 1949). However, this exponent varies greatly and sometimes the resistivity index (RI) curves can be nonlinear in log-log scale. For a sample having a water wettability, the configuration of the conducting phase is a function of porous geometry. The transport properties such as the electrical conductivity and the permeability depend not only on porosity but are also strongly sensitive to the connectivity of the pore space and their micro – geometry (Cerepi et al., 2002). Dunlap et al. (1949) measured *n* varying from 1.5 up to 2.5 in different porous media (sandstones, sand packs, glass beads). Sen (1997) reviewed some experimental results on carbonate rocks containing micro-porosity and attempted to explain the results using effective medium theory. The results from the two studies show that the resistivity becomes anomalously large when the conducting water phase is trapped in isolated regions.

We have analyzed 3 sandstones and 10 carbonates of various porous geometries. They are outcrop rocks, therefore all of them have a water wettability. To measure numerous samples during a short period, we have developed a new measurement method which

combines the centrifuge technique, NMR T_2 relaxation and profile measurement, and electrical measurements. This method allows us to measure six samples at the same time and to follow the drainage of a brine-air system in approximately one week of testing time.
First of all, we describe the rock's porous geometry, then we present our measurement method. At last, we show the experimental results, and a numerical study using random walk simulation.

DESCRIPTION OF POROUS GEOMETRY

We have performed a series of characterization on the porous micro-structure of these samples. It includes X ray micro-tomography, mercury-injection, Scanning Electron Microscopy (SEM) and Nuclear Magnetic Resonance (NMR). The samples are classified into four main rock textures, depending on the pore size, the pore distribution and the pore connection.
Texture I samples are sandstones having a single pore size distribution. The pores are intergranular, with a pore diameter of around 100 μm. Figure 1 shows the SEM image and the mercury - injection of an example of this rock texture, a clean Fontainebleau sandstone.
Texture II samples are carbonates with a single pore size distribution, the pores are intergranular of small size, about 1μm. An example, the Creuë Limestone, is shown in Figure 2.
Texture III samples are carbonates which have a bimodal pore size distribution. It contains two types of pores: the intergranular macro-pores which are well connected, and the intragranular micro-pores. Figure 3 shows an example of the Estaillade Limestone.
Texture IV samples are characterized by macro-pores isolated by micro-pores. An example of the Chassignelles Limestone is shown in Figure 4. More details about the carbonate samples can be found in Fleury et al. (2007). The petrophysical properties of these four textures, like the porosity Φ, the formation factor FF, the permeability K and the cementation exponent m, are presented in Table 1, 2, 3 and 4 respectively.

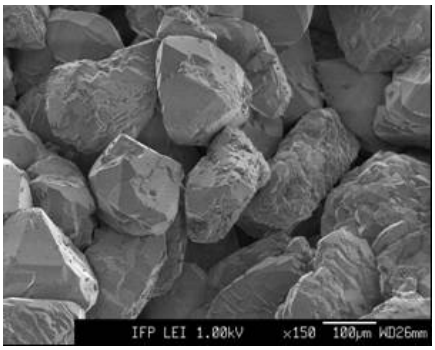

a

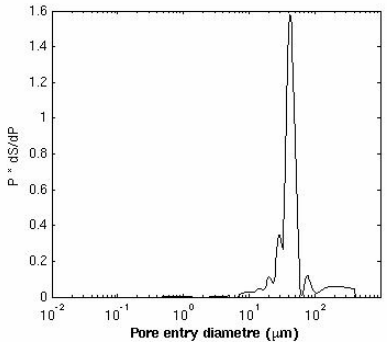

b

Figure 1 : The SEM image (a) shows that Fontainebleau sandstone is composed of quartz grains. The grain diameter is about 200 μm. The grain surface is smooth or coarse. The mercury - injection (b) shows a unimodal pore size distribution.

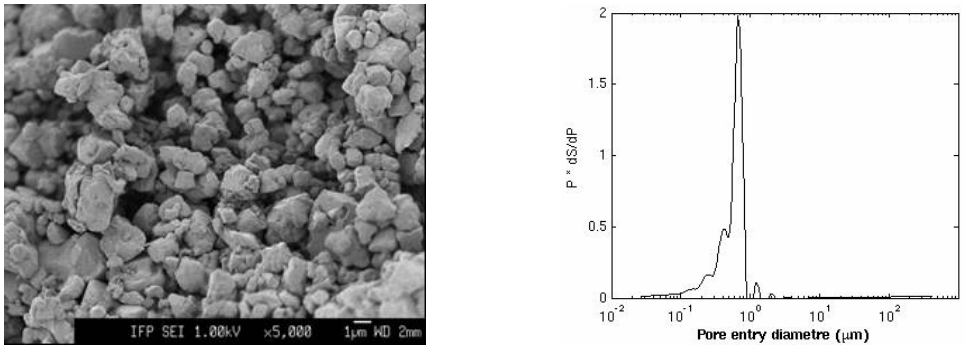

a b

Figure 2 : The SEM image (a) shows that Creuë Limestone is composed of micritical calcite grains. The grain diameter is close to 1 µm. The mercury - injection (b) shows a unimodal pore size distribution .

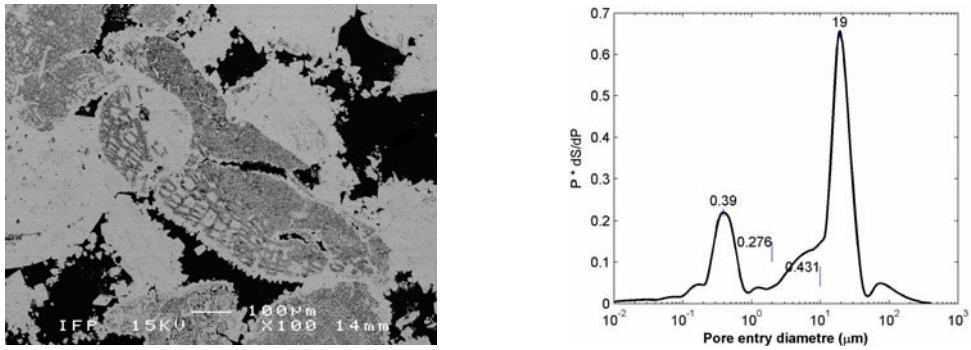

a b

Figure 3 : The SEM image (a) shows that in Estaillade Limestone there are two pore types. The macro-pores are intergranular (black parts); the micro-pores are in some grains (gray parts). There are also the little porous grain in (white parts). The mercury injection data (b) shows a bimodal pore size distribution.

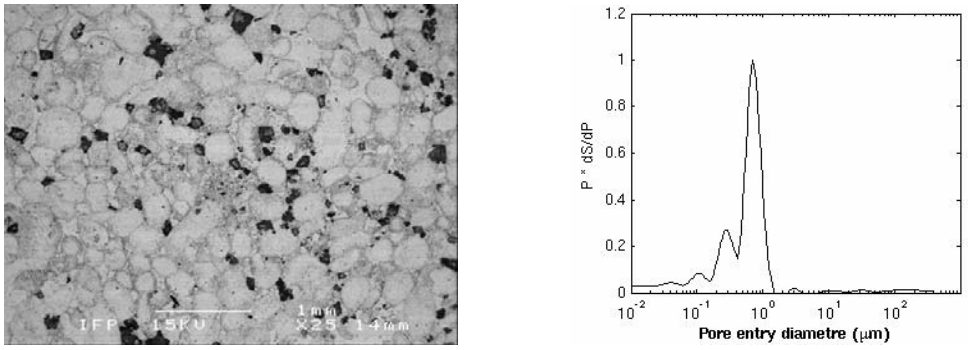

a b

Figure 4 : The SEM image (a) shows that Chassignelles Limestone is composed of two pore types. The macro-pores are isolated (black shaded sections) by the the micro-pores (gray shaded sections). The mercury – injection (b) shows also a bimodal pore size distribution.

EXPERIMENTAL METHODS

The RI - Sw curves were measured in drainage and imbibition for the brine-air fluid system. There are three steps in the experimental procedure: first, the samples are desaturated by centrifugation; then the electrical resistance is measured as well as NMR T_2 distributions and NMR saturation profiles. Then, the sample is centrifuged again at a larger speed of rotation. The NMR spectrometer is a MARAN 2 MHz from Oxford Instruments equipped a 50 mm gradient probe.

Drainage by centrifugation: When a brine saturated sample is centrifuged in air, a pressure gradient is generated by the centrifugal force. This pressure is a function of the position *R* (Figure 5), and is given by:

$$\Delta P(R) = \frac{1}{2}\omega^2\left(R_{\max}^2 - R^2\right)\left(\rho_w - \rho_g\right) \qquad \textbf{(1)}$$

where ω is the rotation velocity, R_{max} is the distance between the rotation center and the outlet face of the plug, ρ_w and ρ_g are the densities of brine and air. In equation (1), we write ΔP and not capillary pressure because no specific attention was paid to reach equilibrium. Theoretically, the maximum pressure is obtained at the inlet face of the plug (Rmin), then it diminishes to zero at the opposite face, where 100% saturation is expected. As a result, there is a saturation profile (Figure 5).

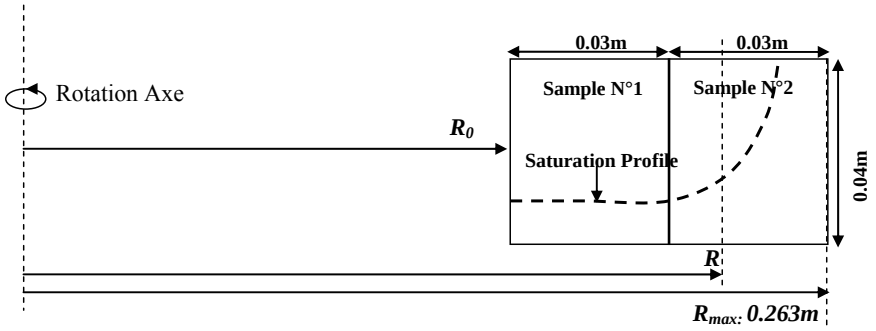

Figure 5 : The position of the sample in the centrifuge.

To avoid strong non-uniform profiles, we superimposed two plugs from the same core and measured separately the resistance and NMR T_2 on each plug. The contact surfaces of the two plugs are smooth and we added a thin water wet membrane between the contact surfaces to insure a capillary continuity. This is important for the interpretation of T_2 distributions, and to some degree for the electrical measurement (discussed later).

Imbibition

After centrifugation, different saturation values were obtained by spontaneous imbibition. The plug was placed in a beaker with the amount of water necessary to reach a given saturation. The uniformity of the saturation profile was controlled by NMR.

Electrical measurements:
The electrical resistance is measured in a core holder cell in which the electrodes are implemented radially around the sample (Figure 6). When the sample is inserted into the cell, a confining pressure of 30 Bar is imposed in order to obtain a good electrical contact.
The design details of the core holder cell as well as a study on the sensitivity of the radial electrode geometry to non – uniform saturation profiles in the porous plate case can be found in Fleury (1998). Essentially, this design strongly attenuates the effect of non-uniform saturation profiles and allows the measurement of continuous RI curves without the need for capillary equilibrium. However, for strong non-uniform profiles, RI values can be underestimated. Therefore, the drainage is performed gradually typically using three pressure steps.
The profiles generated by the centrifuge can be different from the one obtained by porous plate method. In our study, most of our plugs (sample N° 1 in Figure 5) show a uniform profile (Figure 7 a). However, the non –uniform profile appears in Creuë Limestone that could not be avoided (Figure 7 b). We performed also a study about the profile influence using the measured profiles after centrifuge. First, using a 3D finite element simulation reproducing the measurement geometry, we calculated that the local saturation exponent *n* can be underestimated by 5 % when a linear saturation profile ranging from Sw=1 down 0.5 is assumed in the simulation (e.g. the measured *n* would be 1.90 instead of 2). More simply, the effect of non-uniform saturation profiles can also be estimated using a parallel resistance model and the measured saturation profiles. When the saturation difference decreases, the underestimation decreases and becomes negligible.

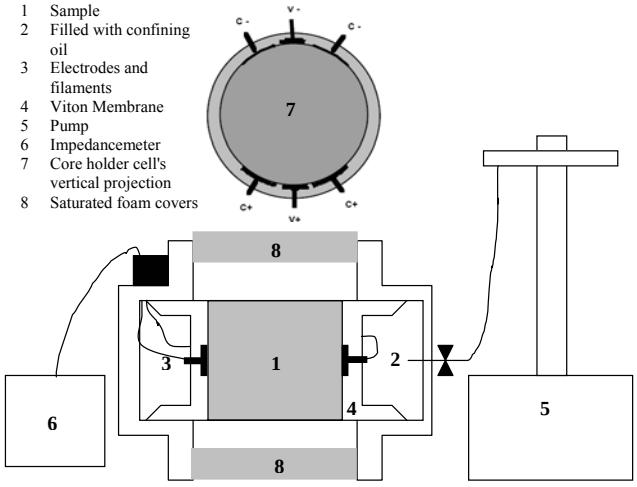

Figure 6 : Schema of the experimental set – up for electrical measurement.

T_2 Distribution , Saturation profile by NMR :
For air-brine systems, the evolution of the T_2 distribution as a function of saturation gives useful information about the drainage or imbibition process in the different pore classes.

For a single pore, the relaxation time T_2 value is proportional to the ratio between the volume of water and the surface wetted by water Wp:

$$\frac{1}{T_2} = \rho_2 \frac{W_p}{V_p Sw_p} + \frac{1}{T_{2B}} \qquad \textbf{(2)}$$

where V_p is the pore volume, Sw_p is the pore saturation and ρ_2 is the surface relaxivity and T_{2B} the brine relaxation time. At Sw=1, the T_2 distribution is related to the distribution of V/S called the " pore size distribution".

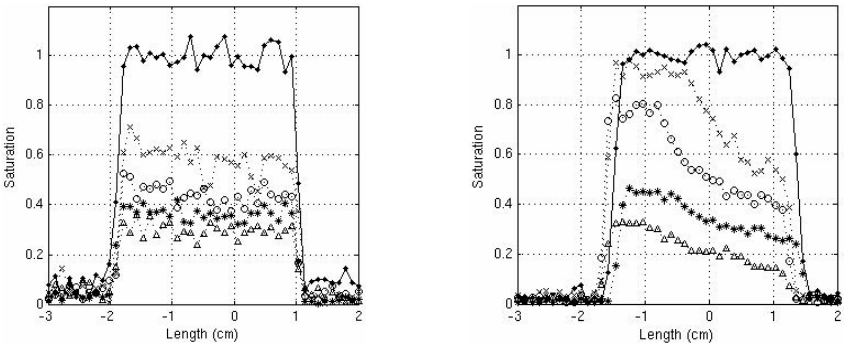

Figure 7 : Saturation profile of a rock sample in the direction of centrifugation at each saturation value in drainage. Each symbol represents a profile at a mean saturation value. a) Rock sample ESTA; b) Rock sample CRE.

At partial saturation for complex porous media containing micro- and macro-pores, we can clarify the drainage or imbibition of these different pore populations. This information is important for the interpretation of the electrical response.
In addition to relaxation measurement, we use a standard NMR 1D imaging technique to observe the saturation profile at each saturation value. From the reference profile measured at Sw=1, the saturation profiles can easily be calculated from the amplitude ratio at a given position (Figure 7). For high permeability samples (Figure 7 a), the profiles are very uniform, whereas for low permeability (0.1 mD, Figure 7 b), a profile still persists despite the use of two superimposed samples. Therefore, the first RI value at Sw=0.75 is slightly underestimated.

RESULTS AND DISCUSSION

We present the RI – Sw measurements of 4 rocks (Fontainebleau Sandstone, Creuë Limestone, Estaillade Limestone and Chassignelles Limestone) whose porous structures have been described in the second section. The fluids used are brine (20g/l NaCl) and air.

Texture I: We have desatured two samples (GF01 and GF02) of the rock Fontainebleau Sandstone until about 3% saturation. The electrical responses of all these plugs are coherent. When the brine saturation is greater than 20%, the curve of resistivity index (Figure 8) plotted versus the average saturation shows an Archie behavior. The saturation

exponent *n* is close to 2. At water saturations below this 20% threshold, we observe a negative deviation and the *n* value diminishes to 1.5. We attribute this deviation to the electrical conduction of the brine film which covers the grain surfaces, as explained later.

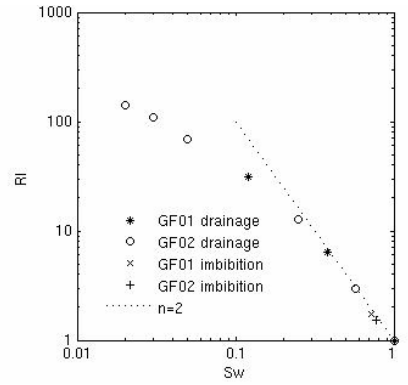

Figure 8 : The RI – SW curve for the Fontainebleau sandstone in drainage.

We have studied the effect of this film conduction by a "random walk" simulation in a dense random packing of spheres (Schwartz 1989, Levitz 1993, Toumelin 2005). The formation factor FF and the resistance index RI can be expressed in terms of the diffusion tortuosity τ_d in the conductive phase as:

$$FF = \frac{\tau_{d(Sw=100\%)}}{\phi} \quad \textbf{(3)}$$

$$RI = \frac{1}{S_w}\left(\frac{\tau_{d(Sw<100\%)}}{\tau_{d(Sw=100\%)}}\right) \quad \textbf{(4)}$$

$$\tau_d = \frac{D(t \to 0)}{D(t \to \infty)} \quad \textbf{(5)}$$

where $D(t\to 0)$ and $D(t\to\infty)$ is the bulk diffusion coefficient and long – time effective diffusion coefficient respectively. In our simulation, thousands of particles released in the brine phase follow a Brownian motion; $D(t\to\infty)$ can be calculated based on the Einstein's relation.

$$\left\langle r^2 \right\rangle(t) = 6D(t)t \quad \textbf{(6)}$$

where $\left\langle r^2 \right\rangle(t)$ is the average displacement of the particles and *t* is their diffusion time. We have, at first, validated our program by computing the Formation Factor on a Random Close Packing of spheres (porosity 38%), as well as on a GF's 3D tomographie X image (porosity 22.9%). The simulations give the formation factor values of 3.8 and 12.9 for the sphere packing and GF tomography image respectively. These simulations values agree well with the theoretical value for sphere packs (3.7) the measured value for the GF sample (11).

To study the film conduction effects, in our simulations, the brine is placed in the form of a continuous film covering the sphere surface. The saturation is increased by raising the

film thickness. The simulation result shows that even with a thin film of thickness about 0.5 µm, the *n* value can be diminished to 1.5, and *n* decreases with the film thickness (see Figure 9).

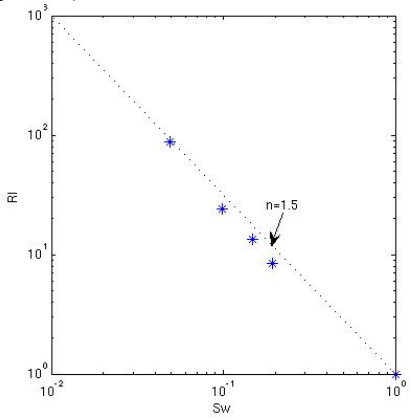

Thickness	S_w	RI	n
0.5 µm	4.9%	87.3	1.5
1.0 µm	9.9%	24.3	1.4
1.5 µm	14.7%	13.4	1.4
2.0 µm	19.4%	8.5	1.3

Figure 9 : Study of the film conduction, curve RI – Sw simulated by random walk method on a Random Close Packing of spheres.

This simulation is a first attempt. A forthcoming study that can reflect the realistic fluid distribution in the porous media and show their influence to the electrical response is on the way and will be published soon.

Texture II: The micritic carbonate Creuë Limestone has an *n* value about 1.6 and we can observe a slight negative deviation. In imbibition mode, the RI – Sw curve in log – log scale is linear. The exponent *n* is about 1.5. Other rocks of the same porous texture show the same electrical behavior.

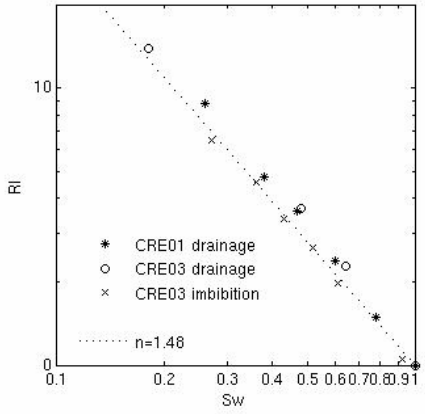

Figure 10 : The RI – SW curve in drainage and imbibition for the sample CRE.

Texture III: The Figure 11 (a) shows the RI – Sw curve of the sample ESTA. It has a non – Archie behavior. We desaturated this sample until 30% of brine saturation. When the brine saturation is smaller than 40%, we observe a positive deviation --- the electrical resistivity and the *n* exponent increases strongly. The T_2 distribution evolution in drainage mode (Figure 12) shows that the macro-pores are drained first during

centrifugation at moderate speed, and the brine is trapped in the micro-pores. Then, at the last rotation step, the brine begins to drain out from the micro-pores.
Interestingly, if we look at the RI – Sw curve measured by Fleury (2002) for the same rock type, we find a same trend in our saturation range (>30%). Fleury used the porous plate method measured the curve down to 5% brine residual saturation. He found a negative deviation between 30% and 5% saturation. The non – Archie behavior is probably due to the micro-pore's repartition in this rock. From the SEM image (Figure 3), we can see that the micro-pores are isolated by the inter-granular pores and by the grains with poorly developed intra-granular micro-porosity. At about 40% saturation, the intergranular macro-pores reach their percolation threshold and the brine is trapped in the intragranular micro-pores. This brine contributes little to the rock's electrical conduction, and therefore the electrical resistance increase quickly as well as the curve shows a positive deviation. However, when the applied pressure increases and the brine saturation is smaller than 30%, these micro-pores begin to be emptied by the brine film covering the grain surface. At this 30% saturation threshold, the brine film electrical conduction become dominant and as a result the exponent *n* diminishes.

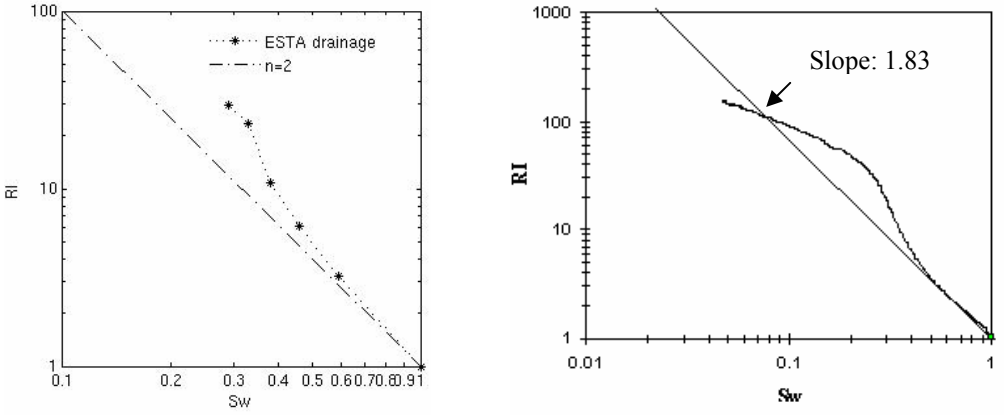

a b

Figure 11 : a) The RI – SW curve in drainage of the sample ESTA. b) The measurement for the same porous texture in drainage by Fleury (2002).

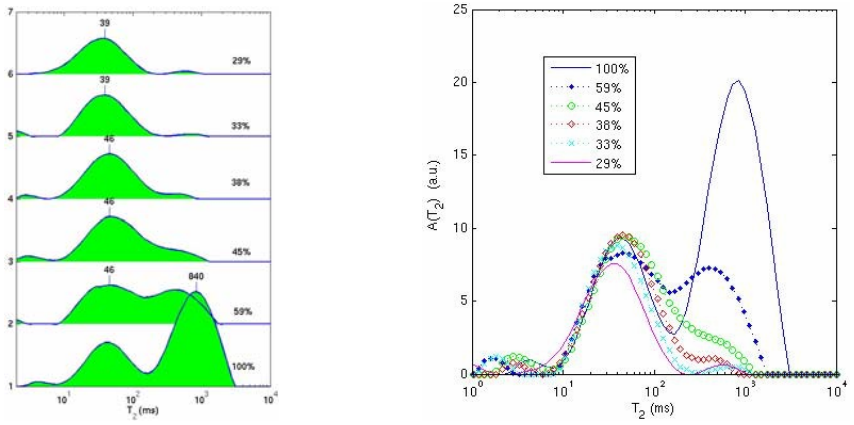

Figure 12 : The T_2 distribution evolution of the rock ESTA in drainage.

Texture IV: We show an example of the plug CHA. These samples have an exponent *n* close to 1.6, and we can observe a slight negative deviation. We find also an electrical hysteresis. The imbibition curve is below the curve in drainage. We look for an explanation in the NMR measurement. During drainage, the macro- and micro-pores are desaturated at the same time, but during imbibition, the macro-pores' peak disappears. This tells us that air is blocked in these macro-pores. The fluids distribution is different in drainage and imbibition and this could be the origin of the hysteresis in this sample.

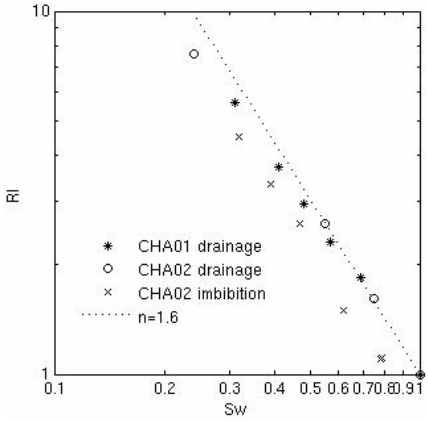

Figure 13 : The RI – SW curve in drainage for the sample CHA.

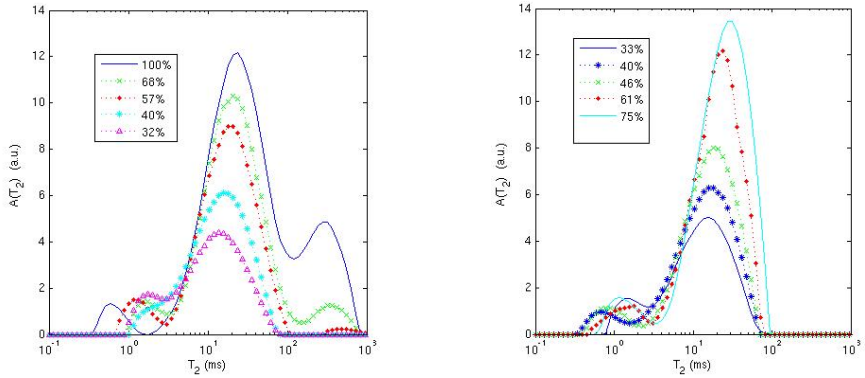

a b

Figure 14 : a) T_2 distribution evolution in drainage for CHA. b) in imbibition.

CONCLUSION

Using a novel experimental technique, we measured the electrical responses of several sandstones and carbonates . The samples are classified in 4 groups according to their pore space structures. We observed different electrical responses for each texture. For the *Texture I*, the RI – Sw curve measured follows an Archie behavior in the saturation range Sw > 20% with an exponent close to 2 and shows a negative deviation at low saturation range (< 20%). We attribute this negative deviation to the water film conduction at low saturation scale. We confirmed the effects of this film conduction by a numerical simulation. For the carbonate samples, the *Texture II* and *IV* often have a small *n* value

as well as a slight electrical hysteresis. The RI – Sw curve of the *Texture III* (bimodal porosity), depends strongly on the micro-porosity configuration. If the micro-pores are isolated, the resistivity can sometimes increase at low saturation values.

PERSPECTIVE

We consider a numerical study to explain the porous structure effects on the electrical response based on our experimental observations. We will model the electrical behavior of our rock samples by "random walk" simulations inside their Xray – tomography 3D images, with a realistic fluid distribution in the porous media.

ACKNOWLEDGMENTS

We are grateful to E. Rosenberg for performing the Xray micro-tomography measurements. We acknowledge also Y. Santerre for providing the set of carbonate samples, and J. Guelard for the MICP measurements. This research is supported by a CIFRE IFP-CNRS grant.

REFERENCES

Archie G. E., "The electrial Resistivity log as an aid in determining some reservoir characteristics", Petroleum Transactions of the AIME, (1942) **146,** 54-62.

Dunlap H. F., Bilhartz H.L, "The relation between electrical resistivity and brine saturation in reservoir rocks", Trans. Am. Inst. Min. Eng, (1949), **186**, 259.

Cerepi A., Burlot R., Galaup S., Barde J – P, Loisy C. and Humbert L., "Effects of porous solid structures on the electrical behaviour : prediction key of transport properties in sedimentary reservoir rock.", Studies in Surface Science and Catalysis, (2002), **144**.

Fleury M., "FRIM: a fast resistivity index measurement method.", Proceedings of the International Symposium of the Society of Core Analysts 14-16 September 1998, The Hague (The Netherlands).

Fleury M., Resistivity in Carbonates: New Insights, Proceeding of the International Symposium of the Society of Core Analysts, 22 – 25 September 2002, Monterey, USA.

Fleury M., Y. Santerre and B. Vincent, Carbonate rock typing from NMR relaxation measurements, Proceeding of the SPWLA Annual Logging Symposium, June, 4-7, 2007.

Levitz P., Knudsen Diffusion and excitation transfer in random porous, J.Phys.Chem., (1993), **Vol 97**, 3813.

Sen P. N., "Resistivity of partially saturated carbonate rocks with microporosity", Geophysics, (1997), **Vol. 62**, No. 2.

Sprunt E. S., "Compilation of electrical resistivity measurements performed by twenty – five laboratories, SCA Survey, (1990).

Schwarts L. M. and Banavar J. R., " Transport properties of disordered continuum systems", Physical Review B, (1989), **Vol 39**, 16, 11965 ~ 11970.

Toumelin E., "Influence of oil saturation and wettability on rock resistivity measurements: a uniform pore – scale approache", SPWLA 46th annual logging symposium, 2005.

Table 1 : Characterization of the rock group « Texture 1 »

Rock name	Sample ID	Φ	FF	M	K (mD)
Fontainebleau Sandstone	GF_01	22.6	10.6	1.6	>1000
	GF_02	21.5	12.4	1.6	>1000
Berea Sandstone	Be_01	19.3	17.0	1.7	192
	Be_02	19.4	16.2	1.7	203
	Be_03	19.4	16.6	1.7	173
	Be_04	19.7	17.2	1.8	184
Clachash Sandstone	CLA_01	21.2	15.1	1.8	322
	CLA_02	21.2	14.3	1.7	300
	CLA_03	21.2	15.0	1.8	293
	CLA_04	21.2	15.1	1.8	261

Table 2 : Characterization of the rock group « Texture II »

Rock name	Sample ID	Φ	FF	m	K (mD)
Creue Limestone	CRE_01	14.5	25.7	2.0	0.5
	CRE_03	13.7	24.6	1.9	0.5
Gudmont Limestone	GUD_01	31.6	20.0	2.2	0.3
	GUD_02	30.0	19.0	2.1	0.3
Oolithe Blanche Limestone	ANS	21.2	22.7	2.1	0.8

Table 3 : Characterization of the rock group « Texture III »

Rock name	Sample ID	Φ	FF	m	K (mD)
Lavoux Limestone	LAV_01	28.7	9.5	1.8	205
	LAV_02	25.2	13.3	1.9	94
	LAV_03	24.8	13.0	1.8	83
Euville Limestone	EUV_01	13.0	59.5	2.0	205
	EUV_02	11.9	63.5	2.0	121
	EUV_03	12.7	51.2	1.9	309
	EUVHAU	13.5	47.3	1.9	1400
Estaillade Limestone	ESTA	23.7	23.9	2.2	273
Brauvillier Limestone	Brau_02	29	30.0	2.8	45
	Brau_03	30	29.0	2.8	58

Table 4 : Characterizations of the « Texture IV »

Rock name	Sample ID	Φ	FF	m	K (mD)
Massangis Limestone	MAS	12.2	147.5	2.4	1.5
Oolithe blanche Chassignelles Limestone	CHA_01	15.7	49.7	2.1	0.1
	CHA_02	14.2	52.0	2.0	0.1
Hauville Limestone	HAU	13.9	75.9	2.2	0.6